Available online at www.sciencedirect.com
ScienceDirect
Geochimica et Cosmochimica Acta 71 (2007) 4327–4341
Geochimica et Cosmochimica Acta
www.elsevier.com/locate/gca

Lithium isotopic systematics of peridotite xenoliths from Hannuoba, North China Craton: Implications for melt–rock interaction in the considerably thinned lithospheric mantle

Yan-Jie Tang [a,*], Hong-Fu Zhang [a], Eizo Nakamura [b], Takuya Moriguti [b], Katsura Kobayashi [b], Ji-Feng Ying [a]

[a] *State Key Laboratory of Lithospheric Evolution, Institute of Geology and Geophysics, Chinese Academy of Sciences, P.O. Box 9825, Beijing 100029, China*

[b] *The Pheasant Memorial Laboratory for Geochemistry and Cosmochemistry, Institute for Study of the Earth's Interior, Okayama University at Misasa, Tottori-ken 682-0193, Japan*

Received 29 August 2006; accepted in revised form 2 July 2007; available online 24 July 2007

Abstract

Li concentrations and isotopic compositions of coexisting minerals (ol, opx, and cpx) from peridotite xenoliths entrained in the Hannuoba Tertiary basalts, North China Craton, provide insight into Li isotopic fractionation between mantle minerals during melt–rock interaction in the considerably thinned lithospheric mantle. Bulk analyses of mineral separates show significant enrichment of Li in cpx (2.4–3.6 ppm) relative to olivine (1.2–1.8 ppm), indicating that these peridotites have been affected by mantle metasomatism with mafic silicate melts. Bulk olivine separates (δ^7Li $\sim +3.3$‰ to $+6.4$‰) are isotopically heavier than coexisting pyroxenes (δ^7Li ~ -3.3‰ to -8.2‰ in cpx, and -4.0‰ to -6.7‰ in opx). Such large variation suggests Li elemental and isotopic disequilibrium. This conclusion is supported by results from *in situ* SIMS analyses of mineral grains where significant Li elemental and isotopic zonations exist. The olivine and opx have lower Li concentrations and heavier Li isotopes in the rims than in the cores. This reverse correlation of δ^7Li with Li concentrations indicates diffusive fractionation of Li isotopes. However, the zoning patterns in coexisting cpx show isotopically heavier rims with higher Li abundances. This positive correlation between δ^7Li and Li concentrations suggests a melt mixing trend. We attribute Li concentration and isotope zonation in minerals to the effects of two-stage diffusive fractionation coupled with melt–rock interaction. The earliest melts may have been derived from the subducted oceanic slab with low δ^7Li values produced by isotopic fractionation during the dehydration of the seawater-altered slab. Melts at later stages were derived from the asthenosphere and interacted with the peridotites, producing the Li elemental and isotopic zoning in mineral grains. These data thus provide evidence for multiple-stage peridotite–melt interaction in the lithospheric mantle beneath the northern North China Craton.

1. INTRODUCTION

Li is a light alkali metal element. The large mass difference (~16%) between its two stable isotopes (^{6}Li $\sim 7.5\%$ and ^{7}Li $\sim 92.5\%$) leads to strong isotopic fractionation during many geological processes, producing overall isotopic variation of >50‰ (Tomascak, 2004). As a mobile element,

* Corresponding author. Fax: +86 10 6201 0846.
E-mail address: tangyanjie@mail.igcas.ac.cn (Y.-J. Tang).

0016-7037/$ - see front matter © 2007 Elsevier Ltd. All rights reserved.
doi:10.1016/j.gca.2007.07.006

Li tends to partition preferentially into the fluid/melt phase during fluid/melt–rock interaction (Brenan et al., 1998b), leading to Li enrichment in differentiated crust relative to the primitive mantle. It is believed that Li^+ and Na^+ can substitute for each other in the M2 site in cpx (Ottolini et al., 2004). Furthermore, Li^+ has a similar ionic radius to that of Mg^{2+} or Fe^{2+}, allowing the substitution of Li for these elements in olivine and pyroxene, potentially charge-balanced by trivalent cations such as Al^{3+}, Fe^{3+}, Cr^{3+}, Sc^{3+}, V^{3+}, and REE^{3+} (Seitz and Woodland, 2000). These characteristics make Li a potential tracer for a number of important mantle processes.

With rapid improvement in analytical techniques and growing interest in light element geochemistry, Li and its isotopes have received great attention in recent years as a potential geochemical tracer for geological processes (Tang et al., 2007) such as the recycling of subducted crustal material (Moriguti and Nakamura, 1998a; Tomascak et al., 2000; Chan et al., 2002a; Elliott et al., 2004; Wunder et al., 2006), mantle partial melting and crystal fractionation (Chan et al., 1992, 1993, 1999; Seitz and Woodland, 2000; Tomascak, 2004; Lundstrom et al., 2005; Teng et al., 2006b), mantle metasomatism or peridotite–melt interaction (Chan et al., 1992, 1993, 1999; Seitz and Woodland, 2000; Woodland et al., 2004; Jeffcoate et al., 2007; Rudnick and Ionov, 2007), and low-temperature alteration (Chan et al., 1992, 2002a; Decitre et al., 2002; Teng et al., 2004; Woodland et al., 2004).

The Li isotopic compositions of fluids, melts, and rocks from subduction-zone settings have been used to probe crust–mantle mass transfer processes. Because seawater has high δ^7Li values (~+31‰), low-temperature seafloor alteration produces seafloor basalts rich in heavy Li relative to fresh MORBs (Chan et al., 1992, 1996, 2002a). Fluids released from subducted-slab metamorphism are variable in composition, depending on the prior history of dehydration, but isotopically heavier than the rocks from which they were released (Tomascak et al., 2002; Elliott et al., 2004). Thus, progressive dehydration of pelagic sediments and altered oceanic crust should produce rocks depleted in the heavy Li isotope relative to seafloor basalt. It has been proposed that subducted eclogite with extremely low δ^7Li values (−11‰) can result from the dehydration of subducted altered oceanic crust (Zack et al., 2003). Recycling of slab residues into the deeper mantle could thus deliver a light Li isotopic component (δ^7Li < 0‰) to the deep mantle. However, this low-δ^7Li signature has not yet been observed in either arc or ocean-island volcanic rocks (+1.4–+11‰; Chan et al., 1992, 2002b; Moriguti and Nakamura, 1998a; Tomascak et al., 1999, 2000, 2002; James and Palmer, 2000; Chan and Frey, 2003; Nishio et al., 2004) except for glass inclusions in olivine from Hawaiian basalts (Kobayashi et al., 2004).

Li isotope geochemistry is a relatively young area of research, and most of the work has been conducted during the last decade. Although previous studies have shed new light on the fluid/melt–mineral interaction at the Earth's surface and into the mantle, many questions remain regarding the Li isotopic compositions of common materials, and the nature and mechanism of Li isotopic fractionation. Data bearing on the Li isotopic systematics in mantle peridotite xenoliths are even more scarce. Therefore, data from these ultramafic rocks and minerals are crucial to our understanding of Li behavior in the mantle.

This paper reports major and trace element and Li isotopic compositions of the well-studied spinel peridotite xenoliths from Hannuoba Tertiary basalts, North China Craton, by means of both multi-collector inductively coupled plasma mass spectrometry (MC-ICP-MS) for bulk mineral separates and *in situ* secondary ionization mass spectrometry (SIMS) analyses, with aims to clarify the distribution of Li in mantle minerals, the inter- and intra-mineral fractionation of Li isotopes during melt–rock interaction, and evaluate the possible geochemical implications of this information.

2. GEOLOGIC SETTING

The North China Craton is one of the world's oldest Archean cratons, preserving crustal remnants as old as 3.8 Ga (Liu et al., 1992). The Late Paleozoic-Early Mesozoic Central Asian orogenic belt bounds the craton to the north, and in the south the Qinling-Dabie and Su-Lu high- to ultra-high-pressure metamorphic belts amalgamated the craton with the Yangtze Craton (Fig. 1). The North China Craton consists largely of Archean to Paleoproterozoic basement (Zhao et al., 2001). Based on differences in geology, tectonic and metamorphic P–T evolution of the basement rocks, the base of the craton can be divided into two distinct blocks, the Eastern and Western Blocks, with the two blocks separated by the Trans-North China Orogen (Zhao et al., 2001) (Fig. 1). Fragments of mélanges, high-pressure granulites and retrograded eclogites have been found only in the Trans-North China Orogen. However, the Late Archean basement of the Eastern and Western Blocks is dominated by Late Archean tonalitic-trondhjemitic-granodioritic gneiss domes surrounded by minor supracrustal rocks. Based on lithology, structure and metamorphic P–T–t paths, Zhao et al. (2001) suggested that the Trans-North China Orogen represents a Paleoproterozoic collisional Orogen along which the Eastern and Western Blocks were sutured at ~1.85 Ga to form the North China Craton.

The North China Craton experienced widespread tectonothermal reactivation during the Late Mesozoic and Cenozoic, as indicated by voluminous Mesozoic granitic and mafic igneous rocks (Zhang and Sun, 2002; Yang et al., 2003; Zhang et al., 2003), Tertiary volcanism (Zhou and Armstrong, 1982), and a change in compositions of mantle xenoliths (Menzies et al., 1993; Griffin et al., 1998). Xenoliths entrained in Ordovician kimberlites occur mainly in Mengyin, Shandong Province, Fuxian and Tieling, Liaoning Province (Fig. 1). These highly refractory xenoliths record the presence of a cold and thick lithospheric keel. In contrast, xenoliths from Tertiary basalts are relatively fertile in mineral compositions.

3. SAMPLE DESCRIPTIONS

The Hannuoba basalts (10–22 Ma) occur as a highland of over 1700 km^2 in the northern margin of the North

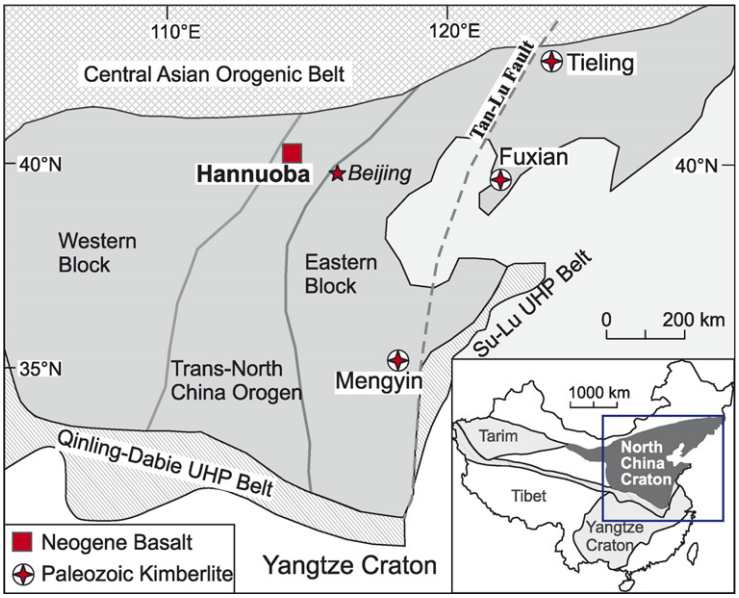

Fig. 1. Tectonic subdivisions of the North China Craton (Zhao et al., 2001) and sample locality. Inset shows location of the craton relative to other blocks and fold belts.

China Craton (Fig. 1). Two series, tholeiitic and alkaline basalts, are intercalated with alkalic basalt dominantly occurring at the base of each sequence. Alkalic basalts host abundant mantle and lower crust xenoliths whereas xenoliths have been found only rarely in the tholeiites (Chen et al., 2001). These xenoliths are mafic to felsic granulites (Chen et al., 2001), spinel and garnet pyroxenites (Song and Frey, 1989; Chen et al., 2001; Xu, 2002; Liu et al., 2005) and abundant spinel peridotites (Song and Frey, 1989; Fan et al., 2000; Chen et al., 2001; Gao et al., 2002; Rudnick et al., 2004; Liu et al., 2005).

In this study, we selected five spinel-facies lherzolites from the Damaping locality in the Hannuoba basalt field for Li content and isotopic analyses. The petrology and geochemistry of spinel peridotite xenoliths from Hannuoba have recently been summarized by Rudnick et al. (2004). The xenoliths chosen for the present study are rounded and range in diameter from 10 to 30 cm. Samples D1 and D5 are coarse-grained and inequigranular (2–3 mm in diameter for most olivines with a few up to 5 mm, 3–4 mm for opxs and ~1 mm for cpxs), and show a transitional texture between coarse and porphyroblastic. Samples D2 and D3 are massive and coarse- to medium-grained (1–3 mm in diameter for most grains), with granular to granuloblastic textures. Their opx, cpx, and spinels are often connected to form aggregates. Sample D4 shows a porphyroclastic texture, and their minerals are elongated to form very weak foliation. The mineral grains in sample D4 are slightly smaller than those in D2 and D3, most olivines and opxs are about 1–2 mm in diameter, with a few up to 3 mm. Cpx grains are <1 mm in diameter. Some elongated spinels are 1–2 mm, and rounded spinels are less than 1 mm. Large olivine grains are usually kink-banded, indicative of high temperature plastic deformation.

The rocks are generally fresh except for samples D3 and D4, which show variable serpentinization of olivines along grain boundaries and fractures, but the degree of alteration is very weak in the interior of these two xenoliths. The mineral mode for these lherzolites is variable (ol = 55–66%; opx = 20–30%; cpx = 8–15%; sp = 1–2%), but with most samples having a relatively high modal percentage of opx and a low modal percentage of cpx (Appendix A). Both cpx and opx in these samples are homogeneous and free from exsolution lamellae. Most spinels have vermicular shapes and occur as interstitial phases at the grain boundaries of other minerals. Some rounded spinels are included in orthopyroxene grains.

4. ANALYTICAL METHODS

All of the clean room procedures, including the wet chemical treatments and trace element and Li isotope analyses, were undertaken at the Pheasant Memorial Laboratory (PML) for Geochemistry and Cosmochemistry, Institute for Study of the Earth's Interior, Okayama University at Misasa, Japan (Nakamura et al., 2003).

Fresh xenoliths were first cut, crushed and then sieved with stainless steel sieves (180–250 μm). Olivine, opx and cpx were separated by handpicking under a binocular microscope, resulting in a purity of >99%. These separates were then cleaned in an ultrasonic bath in Milli-Q water (>18.0 MΩ cm) for 15 min. In order to remove any possible contamination in these separates, the following washing and leaching with HCl were undertaken. Olivine separates were washed with 0.5 M HCl for 30 s, and then rinsed three times using Milli-Q water. Cpx and opx separates were leached with 6 M HCl for 12 h in an ultrasonic cleaner, and then rinsed three times using Milli-Q water. This leaching

process was undertaken repeatedly until the HCl leaching solution was colorless. Generally, two leaching treatments were sufficient. After drying at 110 °C, the mineral separates were ground into powders using a silicon nitride mortar. Approximately, 20 mg aliquots of these powders were weighed and dissolved for both trace element and Li isotopic analyses.

It is well known that HCl can dissolve olivine and silicate glasses, and form secondary amorphous silica (e.g., Tanaka and Nakamura, 2005). If a large amount of Li is partitioned into the newly formed amorphous silica, the influence of Li isotopic contamination must be considered. In order to evaluate the distribution of Li into the amorphous silica in HCl leaching processes, the distribution coefficient between amorphous silica and 6 M HCl was determined by the following experiment. 100 mg of olivine powder (Li = 1.8 ppm) was used to form amorphous silica by HCl dissolution. The HCl was doped with 2 μg of Li before dissolution in order to detect by ICP-MS analysis (Moriguti et al., 2004) Li partitioned into the amorphous silica from the HCl. Subsequently, the olivine was dissolved completely by 6 M HCl to form amorphous silica. The amount of Li in the newly formed amorphous silica was determined, and the distribution coefficient of Li between amorphous silica and HCl was found to be quite small ($D_{\text{amorphous silica–HCl}} = 0.003$). That is, the influence of this 0.3% of Li included in dissolved materials by HCl, partitioned into amorphous silica, is negligible to the Li isotope ratio of undissoluted materials such as pyroxenes. Thus the HCl leaching processes have negligible effect on the original Li isotopic composition of the pyroxenes in this study.

4.1. Major and trace elements

Major element oxide analyses of the minerals were carried out on polished thin sections at the State Key Laboratory of Lithospheric Evolution, Institute of Geology and Geophysics, Chinese Academy of Sciences, using a CAMECA SX51 electron probe micro-analyzer (EPMA). Analyses were performed with a 15 kV accelerating voltage and a 20-nA beam current. Natural and synthetic glasses were used for standard calibration and all matrix corrections were made using the CAMECA PAP correction program. Modal mineralogy of the peridotites was determined by point counting techniques and major element compositions of whole rocks were obtained from mass balance calculation using the mineral compositions (Table 1) and modal mineralogy (Appendix A). Furthermore, the olivines and pyroxenes from D4 and D5 were also examined using SEM-EDX to check for the variation of major element compositions after *in situ* Li isotope analyses by SIMS at the PML following the procedure described in Kobayashi et al. (2004).

The procedures for determination of all trace element compositions of pyroxenes and Li contents of olivine followed Makishima and Nakamura (2006) and Moriguti et al. (2004) using ICP-MS. Analytical reproducibility was typically better than 5% (RSD) for most of the trace elements. During the course of this study, replicate analyses of GSJ JB-3 showed <3% difference from those in Makishima and Nakamura (2006) and Moriguti et al. (2004). The results are shown in Table 2 and Appendix B.

4.2. Li separation and isotope analysis by MC-ICP-MS

The analytical procedure for chemical separation of Li followed Moriguti and Nakamura (1998b). The resulting Li fraction after column chemistry was dissolved in 0.5 M HNO_3 to produce a 10 ppb Li solution. No other elements were observed in these sample solutions, and the recovery yield was in excess of 99.2%.

Lithium isotope measurements were undertaken using a Thermo-Finnigan Neptune MC-ICP-MS equipped with nine Faraday cups and multi-ion counting collectors. The accelerating voltage was 10 kV. The Faraday cup collectors are fitted with 10^{11} Ω resistors allowing detection of ion currents of 10^{-14} to 5×10^{-10} A. The operating conditions are presented in Appendix C. Solutions were introduced into the Ar plasma through an Aridus desolvator (Cetac Technology, USA). $^6Li^+$ and $^7Li^+$ signals were measured simultaneously in static mode. The integration and idling times for the two mass peaks were 4.194 and 3.000 s, respectively. Gain calibration and baseline measurements were undertaken once a day.

Sample analyses were bracketed by analyses of a solution prepared from the NIST L-SVEC standard in order to achieve normalized isotopic compositions as performed in Tomascak et al. (1999). The $^7Li^+$ signal obtained for the 10 ppb standard solution was typically 12–15 V. In each data acquisition, 55 ratios were collected in approximately 4 min. After acquisition of data for the standard and sample, the sample introduction system of the MC-ICP-MS was washed for 150 s using 0.5 M HNO_3.

Before each standard and sample measurement, background was measured for approximately 8 min (112 scans) using 0.5 M HNO_3. $^7Li^+$ signal of ~100 mV was observed in the background measurement. Both the $^6Li^+$ signal and the $^7Li^+$ signal decreased gradually with time. This decay was typically 2.5 mV/min ($^7Li^+$), but $^7Li/^6Li$ ratios did not change systematically. In order to correct for the background in each standard and sample analysis, the intensities of $^7Li^+$ and $^6Li^+$ for the background were extrapolated by curve fitting to the time of the data acquisition for the standard and sample analyses. For each analysis of the standards and samples, the calculated intensities of $^7Li^+$ and $^6Li^+$ of the background were subtracted and the mean value of the corrected $^7Li^+$ and $^6Li^+$ signal was used to obtain the $^7Li/^6Li$ ratio. The $^7Li/^6Li$ ratio for the samples was normalized to the averaged $^7Li/^6Li$ of the standards before and after the sample analysis. Data are represented as deviations in parts per thousand of the $^7Li/^6Li$ from that of the standard (δ^7Li). Analytical precision was <0.06‰ (2σ mean). The difference between the δ^7Li of the two standards bracketing each sample was typically <0.4‰ and averaged ~0.2‰.

Five separate analyses were undertaken for seawater from the Mariana Trough, W34-5 (20°58.99′N, 143°24.68′E, 4871 m depth) and standard rock sample, GSJ JB-2. δ^7Li values of the seawater and JB-2 were

Table 1
Major-element composition (wt%) of mineral phases in spinel peridotites (average value of (*n*) analyses)

Mineral:	Olivine					Opx				
Sample:	D1	D2	D3	D4	D5	D1	D2	D3	D4	D5
n	4	4	4	4	4	4	4	4	4	4
SiO_2	40.50	41.22	41.13	41.00	41.34	54.80	54.79	55.02	55.36	55.59
TiO_2						0.18	0.14	0.06	0.10	0.25
Al_2O_3						4.97	4.78	4.63	4.25	3.87
Cr_2O_3						0.20	0.42	0.36	0.33	0.34
MgO	48.81	48.19	48.11	48.01	48.97	32.41	32.05	32.30	32.54	32.91
CaO	0.08	0.09	0.07	0.06	0.04	0.73	0.74	0.70	0.57	0.47
MnO	0.14	0.17	0.13	0.09	0.10	0.09	0.10	0.15	0.14	0.16
FeO	10.66	10.23	10.10	10.08	9.52	6.51	6.41	6.28	6.58	5.69
NiO	0.35	0.35	0.41	0.40	0.34	0.10	0.12	0.11	0.05	0.11
Na_2O						0.06	0.10	0.11	0.09	0.07
Mg#	89.2	89.5	89.6	89.6	90.3	90.0	90.0	90.3	90.0	91.2
Mineral:	Cpx					Spinel				
Sample:	D1	D2	D3	D4	D5	D1	D2	D3	D4	D5
n	4	4	4	4	4	2	2	2	2	2
SiO_2	51.50	52.26	52.02	52.09	52.62					
TiO_2	0.79	0.44	0.50	0.52	0.26	0.18	0.16	0.19	0.07	0.07
Al_2O_3	7.42	6.55	6.75	6.55	5.81	56.10	56.37	55.94	58.34	52.46
Cr_2O_3	0.41	0.76	0.86	0.79	1.12	8.51	10.99	11.67	9.53	15.71
MgO	14.79	15.07	14.97	14.92	15.08	21.10	20.05	19.97	20.29	19.67
CaO	19.69	20.03	19.82	20.49	20.67					
MnO	0.04	0.12	0.12	0.09	0.13	0.04	0.12	0.05	0.09	0.07
FeO	2.86	2.28	1.79	1.64	1.57	10.52	9.53	9.76	9.43	9.45
NiO						0.45	0.36	0.39	0.40	0.34
Na_2O	1.99	1.70	1.85	1.76	1.73					
Cr#						9.2	11.6	12.3	9.9	16.7
Mg#	90.3	92.3	93.8	94.3	94.6	78.3	79.1	78.6	79.5	79.0

Mg# = 100 × molar $Mg^{2+}/(Mg^{2+} + Fe^{2+})$; Cr# = 100 × molar Cr/(Cr + Al). Blank is below detection limit. Abbreviations: opx, orthopyroxene; cpx, clinopyroxene.

+31.00 ± 0.43‰ (2σ, $n = 5$) and 5.02 ± 0.45‰ (2σ, $n = 5$), respectively, consistent with values obtained by TIMS, within analytical error (+30.0 and +4.9‰, ±0.7‰ 2σ reproducibility) of the seawater and JB-2, respectively (Moriguti and Nakamura, 1998b).

4.3. *In situ* Li isotope analysis by SIMS

Thin sections for D4 and D5 were polished and cleaned with diluted HF and HNO_3 followed by water, and subsequently dried in an oven and gold-coated for SIMS analysis. *In situ* Li concentrations and isotopic compositions were measured by a CAMECA ims-5f and a CAMECA ims-1270 ion probes, respectively, following the procedures described in Kobayashi et al. (2004). Lithium concentration was calculated from intensity ratios of $^7Li^+/^{30}Si^+$ calibrated standard clinopyroxene KLB-1 (Li = 1.37 ppm). Typical reproducibility using the standard cpx was 1.5% (RSD, $n = 10$). During the Li isotope analyses, data acquisition was undertaken by peak jumping with a single electron multiplayer using magnetic switching. In order to avoid correction for matrix effects, an olivine from SanCarlos (MW-sc; $\delta^7Li = -2.27$‰, Li = 1.46 ppm) and a clinopyroxene from Malaita, Solomon island (SAE152; $\delta^7Li = +1.74$‰, Li = 4.85 ppm) were used as standards. Typical reproducibilities of the isotope analysis using standard olivine and cpx were 1.2 and 1.3‰ (RSD, $n = 5$), respectively.

5. RESULTS

5.1. Elemental geochemistry

Comparisons of core and rim analyses by EPMA and SEM-EDX demonstrated that the minerals in these peridotites are homogeneous in major oxides. As summarized by Rudnick et al. (2004), the minerals in the Hannuoba xenoliths are similar in composition to those in off-craton spinel peridotite xenoliths worldwide but differ significantly from those in cratonic peridotites (Fig. 2). The differences are primarily in bulk rock and mineral compositions, rather than pressure (garnet vs. spinel) or temperature. We selected the 2-pyroxene thermometer of Brey and Köhler (1990) to calculate the equilibration temperatures for these xenoliths. If a pressure of 1.5 GPa is assumed, the estimated equilibration temperatures are 1049, 1055, 1053, 981, and 968 °C for D1, D2, D3, D4, and D5, respectively.

Table 2
Trace element compositions (ppm) of cpx

	Sample				
	D1	D2	D3	D4	D5
Rb	0.015	<0.004	0.013	0.006	0.015
Ba	0.067	0.067	0.013	0.098	0.080
Th	0.019	0.031	0.011	0.019	0.049
U	0.006	0.012	0.004	0.006	0.014
La	1.03	0.765	0.566	0.382	1.34
Ce	3.96	2.94	2.44	1.71	3.57
Pb	0.112	0.096	0.051	0.049	0.060
Pr	0.755	0.573	0.537	0.374	0.475
Sr	71.5	61.3	58.7	41.5	59.6
Nd	4.65	3.63	3.70	2.74	2.31
Sm	1.77	1.45	1.54	1.28	0.783
Eu	0.724	0.623	0.655	0.551	0.325
Gd	2.52	2.22	2.34	2.08	1.25
Tb	0.505	0.445	0.474	0.441	0.268
Dy	3.42	3.09	3.25	3.10	2.03
Y	21.9	20.6	21.2	20.5	13.6
Ho	0.765	0.699	0.722	0.722	0.478
Er	2.02	1.88	1.96	1.93	1.33
Tm	0.302	0.291	0.291	0.300	0.207
Yb	1.97	1.95	1.92	2.02	1.34
Lu	0.263	0.268	0.267	0.271	0.185
ΣREE	24.7	20.8	20.7	17.9	15.9
$(La/Yb)_N$	0.36	0.27	0.20	0.13	0.69

5.2. Bulk Li concentrations and isotope ratios of mineral separates

Li and other trace elements measured in cpx, normalized to primitive mantle (McDonough and Sun, 1995), are plotted in Fig. 3b. All cpx shows depletion in Li relative to the HREE. Clear variations in Li concentrations have been observed between mineral phases (Table 3). In these samples, bulk Li contents in olivine (1.2–1.8 ppm) are lower than those in pyroxenes. Cpx has the highest Li concentrations (2.4–3.6 ppm), followed by opx (1.4–2.2 ppm). Seitz and Woodland (2000) established a general Li partitioning relationship in equilibrated peridotites: ol > cpx ⩾ opx ≫ sp. The Hannuoba peridotite xenoliths show Li partitioning that deviates from this ordering, showing enrichments of Li in cpx relative to concentrations in olivine (Fig. 4).

MC-ICP-MS data show δ^7Li values in a range from +3.3‰ to +6.4‰ in olivine, from −4.0‰ to −6.7‰ in opx, and from −3.3‰ to −8.2‰ in cpx in these xenoliths (Table 3). For each sample, olivine has the heaviest δ^7Li. Cpx has slightly lower δ^7Li than coexisting opx, with one exception in D4, in which opx has δ^7Li lower than that of cpx (Fig. 5). These lower δ^7Li for pyroxenes are within the range for Trescolmen eclogites (−11‰ to +5‰) reported in Zack et al. (2003).

5.3. *In situ* analyses of concentration and isotopic compositions of Li by SIMS

All Li SIMS data are summarized in Table 4 and are plotted in Figs. 6–8. Large variations in Li concentrations and isotope ratios are observed within individual mineral grains of the peridotite xenoliths. A profile analysis across a ~2 mm diameter olivine from D4 shows clear Li elemental and isotopic zonation ranging from 1.1 to 1.8 ppm and from 14.6‰ to 1.2‰ δ^7Li from the

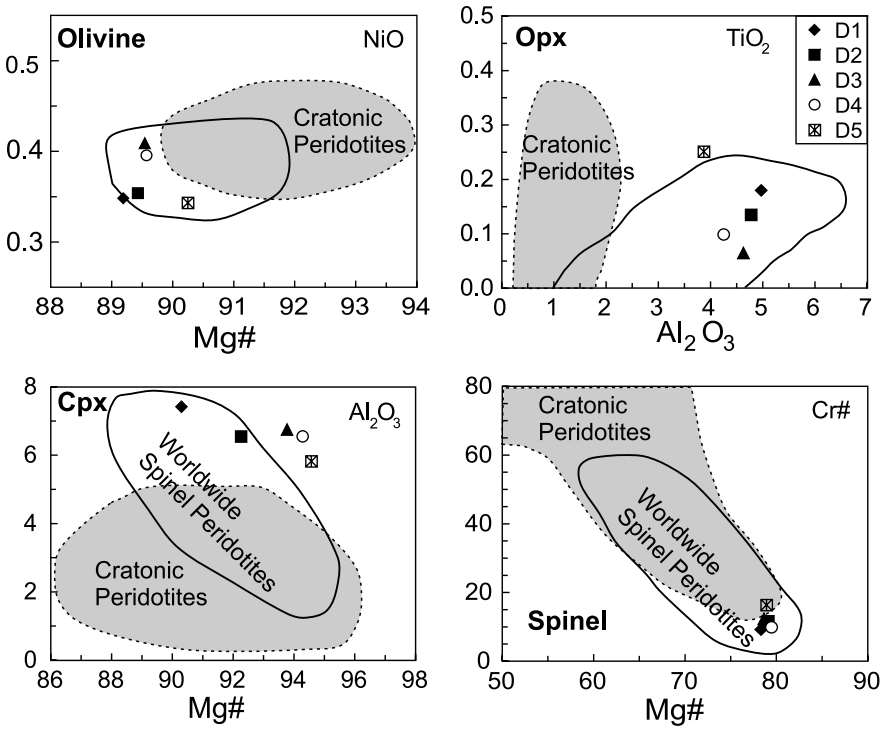

Fig. 2. Mineral compositional plots for the Hannuoba peridotites. Open field is for off-craton spinel peridotites, worldwide and grey field encompasses minerals from cratonic peridotites (including Kaapvaal, east Greenland, Siberia, and Tanzania) (Rudnick et al., 2004).

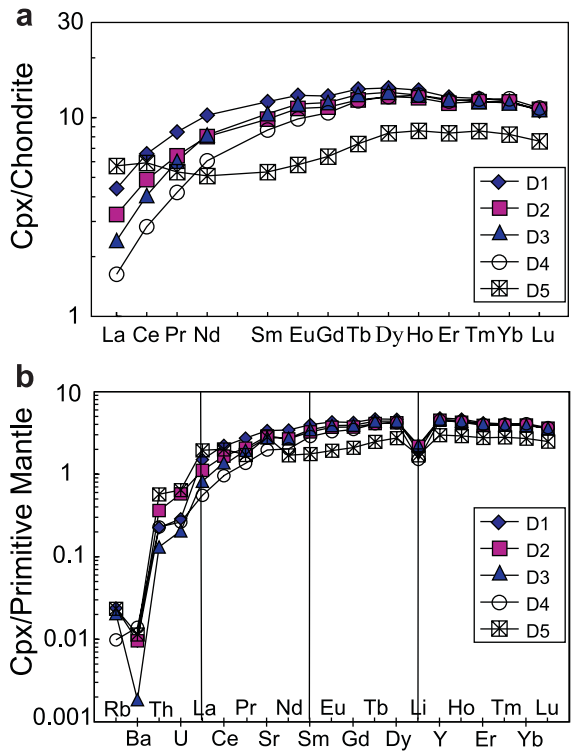

Fig. 3. Chondrite-normalized REE patterns (a), and primitive mantle-normalized spidergram (b) for cpx from the Hannuoba peridotites. Data for chondrite and primitive mantle are from Anders and Grevesse (1989) and McDonough and Sun (1995), respectively.

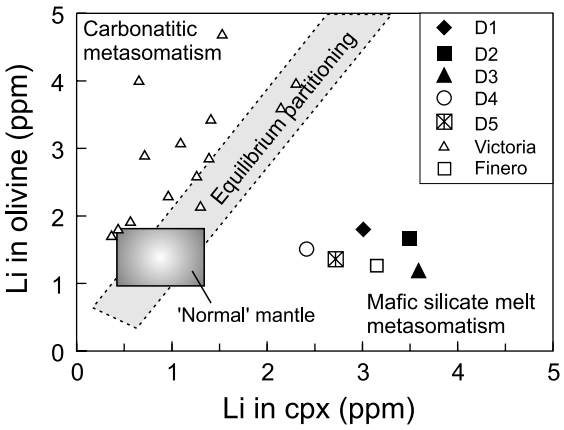

Fig. 4. Li–Li diagram showing Li abundances in coexisting cpx and olivine. Li concentrations in 'normal' mantle, i.e., fertile to moderately depleted peridotites, are from Seitz and Woodland (2000). The dashed field represents equilibrium partitioning. Data for Victoria and Finero samples are from Woodland et al. (2004) and Seitz and Woodland (2000), respectively.

rim to the core, respectively (Fig. 6a and c). A similar pattern of isotopic zonation is observed in a 600 μm cpx from the same sample (Fig. 6b and d), although Li elemental zonation is opposite to the coexisting olivine. A 700 μm opx also from D4 (Fig. 6b and e) has a similar pattern of elemental and isotopic zonation to that observed in the olivine (Fig. 6c). In comparison to olivine and cpx, the magnitude of Li elemental and isotopic zoning in the opx is much larger, with Li concentration and δ^7Li ranging from 2.4 to 0.3 ppm and −13.9‰ to 6.6‰ from the core to the rim, respectively.

In sample D5, an olivine (Fig. 7a and e) shows a similar pattern of elemental and isotopic zonation to that observed in the D4 olivine. However, two opx grains show different styles of zonation. The zoning pattern of the opx-2 in D5 (Fig. 7h) is similar to the pattern observed in D4 opx. Although the opx-1 in D5 (Fig. 7g) has a similar Li elemental zonation to that observed in opxs from other samples (Figs. 6 and 7), its δ^7Li values vary from 8‰ at one side to 0‰ at another side, which is distinct from the δ^7Li zoning in the other opx. A 500 μm diameter cpx from D5 (Fig. 7b) also shows a similar pattern of zonation as observed in D4 cpx (Fig. 6d).

In summary, all the olivine and opx grains examined by SIMS (except D5 opx-1) show significant zonation of Li concentration and isotopic ratios. The cores have higher Li concentrations but lower δ^7Li ratios, and the rims have lower Li abundances but higher δ^7Li. However, the Li element zonation in cpxs is opposite to the patterns for the olivines and opxs; and the cpxs show higher Li concentrations and δ^7Li in the rims than those in the cores. In addition, the pyroxenes, especially opx grains, have large variable Li concentrations and δ^7Li and have lower δ^7Li and higher Li concentrations than coexisting olivines.

6. DISCUSSION

6.1. Bulk Li enrichment and peridotite–melt interaction

Depletions in LREE (Fig. 3a) and highly incompatible elements, in particular the mobile elements Rb, U, and Ba

Table 3
Li concentrations and isotopic compositions of mineral separates measured by MC-ICP-MS

Sample	Ol			Opx			Cpx			Bulk
	Li (ppm)	δ^7Li	2σ	Li (ppm)	δ^7Li	2σ	Li (ppm)	δ^7Li	2σ	δ^7Li
D1	1.80	3.34	0.05	2.20	−6.67	0.02	3.01	−8.25	0.02	−0.14
D2	1.66	6.39	0.05	1.75	−5.01	0.03	3.49	−5.59	0.05	2.44
D3	1.19	5.37	0.05	1.64	−3.98	0.03	3.59	−5.32	0.04	1.60
D4	1.51	5.35	0.04	1.37	−5.27	0.05	2.41	−3.25	0.06	0.94
D5	1.37	5.20	0.04	1.89	−4.35	0.05	2.72	−7.54	0.05	1.28

Abbreviations: ol, olivine; opx, orthopyroxene; cpx, clinopyroxene. Bulk reconstructed δ^7Li calculated using modal analyses in Appendix A.

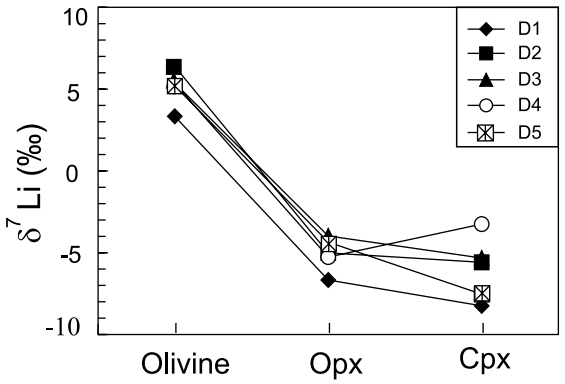

Fig. 5. Plots showing the systematic differences in δ^7Li between olivine, cpx, and opx.

(Fig. 3b), in most of the peridotites suggest that these rocks have experienced partial melting. The negative Li anomaly in cpx (Fig. 3b) could reflect the preference of olivine to incorporate Li relative to REE.

Seitz and Woodland (2000) reported that the compositional ranges of Li in olivine and pyroxenes in fertile to moderately depleted mantle are 1–1.8 ppm and 0.5–1.3 ppm, respectively. The high Li contents in the Hannuoba lherzolites (e.g., 2.4–3.6 ppm for cpx, Table 3) suggest, therefore, that these samples have been enriched by additional processes (metasomatism). The concave REE pattern in D5 (Fig. 3a) also appears to indicate enrichment in LREE after melt extraction. However, this later enrichment process had no significant effect on the Li enrichment because the Li content of D5 is similar to that in other samples, indicating the decoupling of Li and other incompatible elements due to its greater diffusivity.

The distribution of Li between cpx and olivine can best be viewed in a simple Li–Li plot (Fig. 4). All of the Hannuoba samples plot outside the range for 'normal' mantle defined by Seitz and Woodland (2000), and plot far from the empirical region indicating equilibrium partitioning of Li between cpx and olivine [D_{Li} (ol/cpx) = 1.3] (Brenan et al., 1998a), perhaps reflecting the metasomatic processes that have affected these samples. The preferential Li enrichment in cpx relative to olivine in these peridotites (Fig. 4), similar to the peridotite from Finero, Italy, which also exhibits enrichment in Li in cpx relative to olivine, possibly indicates that the metasomatic agent was mafic silicate melt (Seitz and Woodland, 2000). However, most of the samples from Victoria, Australia, plotting to the left side of the diagram (Fig. 4), show the influence of intrusion with carbonatitic melts (Woodland et al., 2004). From available cpx-fluid experimental partitioning data (Brenan et al., 1998a,b), it cannot be ruled out that the metasomatizing agent was a fluid.

The compositional zonation in olivine xenocrysts entrained in the Early Cretaceous Fangcheng basalts in Shandong Province, China, also provides evidence for peridotite–melt reaction beneath the southeastern portion of the North China Craton (Zhang, 2005). Similarly, Liu et al. (2005) suggested that garnet pyroxenite veins in composite xenoliths from the Hannuoba basalts are the products of peridotite–melt reaction. This peridotite–melt

Table 4
In situ analytical data by SIMS

Point	Distance (μm)	Li (ppm)	δ^7Li	2σ
D4_Ol				
P1	61	1.05	14.6	0.8
P2	306	1.78	1.2	0.7
P3	612	1.78	3.8	0.7
P4	857	1.76	2.8	0.7
P5	1204	1.76	3.0	0.7
P6	1429	1.76	3.9	0.6
P7	1673	1.75	4.1	0.7
P8	1939	1.60	3.7	0.8
P9	2153	1.14	6.7	0.8
D4_Opx				
P1	36	0.34	6.6	1.5
P2	68	1.45	1.6	0.8
P3	208	1.97	−2.2	1.0
P4	318	2.14	−12.5	0.8
P5	438	2.37	−13.9	0.8
P6	552	2.16	−2.3	0.9
P7	635	1.84	−0.5	1.0
P8	708	0.39	4.0	1.6
D4_Cpx				
P1	31	2.79	−4.5	0.9
P2	78	2.70	−6.6	1.0
P3	286	2.40	−7.3	0.8
P4	427	2.54	−6.7	0.9
P5	495	2.65	−4.1	0.9
P6	604	3.13	−0.1	0.8
D5_Ol-1				
P1	102	1.11	8.5	0.8
P2	286	1.51	4.4	0.8
P3	510	1.56	3.3	0.8
P4	735	1.54	2.8	0.8
P5	939	1.52	4.1	0.6
P6	1143	1.59	2.8	0.6
P7	1316	1.58	3.5	0.7
P8	1480	1.14	12.1	0.8
D5_Opx-1				
P1	21	0.28	8.2	2.1
P2	168	0.80	8.3	1.1
P3	307	1.16	6.6	1.0
P4	441	1.25	7.9	0.8
P5	601	0.82	4.1	0.9
P6	769	0.20	−0.1	2.1
D5_Opx-2				
P1	51	0.39	−7.0	2.0
P2	510	1.81	−18.3	0.8
P3	1010	2.17	−20.0	0.9
P4	1510	2.40	−22.4	0.8
P5	1837	1.70	−18.7	0.8
P6	2143	0.95	−6.2	1.3
D5_Cpx-1				
P1	45	2.91	−4.7	1.1
P2	172	2.54	−6.8	1.2
P3	313	2.34	−10.3	1.3
P4	424	2.40	−9.5	1.4
P5	505	2.46	−1.0	1.3

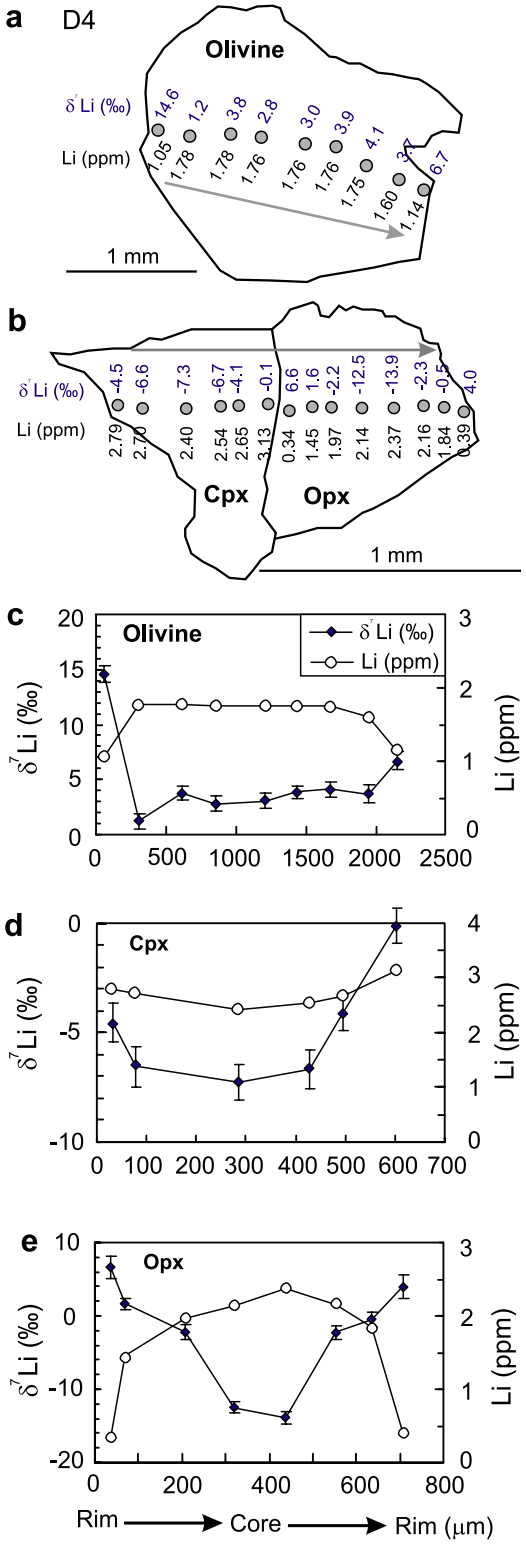

Fig. 6. Outlines of olivine (a), cpx and opx (b) crystals from the D4 showing the position of the Li isotopic and Li concentration measurements by SIMS. (c), (d), and (e) are corresponding plots of Li isotope and concentration as profiles across the crystals.

reaction could also have been responsible for the enrichment of Li in these peridotites.

6.2. Li isotopic fractionation during peridotite–melt interaction

There are three factors that can result in a large difference in Li isotopic compositions between olivine and pyroxenes. They are (1) high temperature fractionation of δ^7Li between mineral phases (Seitz et al., 2004), (2) diffusion-driven fractionation (Teng et al., 2006a), and (3) mixing with low δ^7Li melt (Nishio et al., 2004), which was perhaps derived from a process approximating Rayleigh distillation (Zack et al., 2003) or a combined process of alkali diffusion and melt extraction (Lundstrom et al., 2005). In this section, we evaluate each and provide our impression of which process was the most important.

6.2.1. Isotopic fractionation at high temperature

There are large differences in δ^7Li between the coexisting olivine and pyroxene in the Hannuoba peridotites (9–13‰ based on bulk mineral data and >30‰ based on *in situ* data). Because these peridotites have experienced partial melting and subsequent mafic silicate melt metasomatism, the possibility of fractionation of Li isotopes during these processes should be considered. At temperatures of magmatic processes, Li isotopes do not show per mil-level mass fractionation (Tomascak et al., 1999), indicating that such high temperatures cannot promote a significant fractionation at equilibration. This conclusion has been supported by the constant isotopic values of bulk rocks and olivine separates from basaltic lavas (Chan and Frey, 2003; Jeffcoate et al., 2007). Although isotopic fractionation at high temperature has been suggested by Seitz et al. (2004), the difference is small (~2‰, just beyond analytical uncertainty). Also, the equilibrium fractionation factors for temperatures of 950–1160°C indicate little or no fractionation and this has been confirmed by the study of igneous systems equilibrated at the same temperatures (Tomascak et al., 1999; Chan and Frey, 2003; Bryant et al., 2004; Teng et al., 2004, 2006b). Experimental results indicate that Li isotopic fractionation between mantle minerals and fluid at temperatures >900 °C is <1.0‰ (Wunder et al., 2006), much smaller than the differences in isotopic composition in our samples. Thus, Li isotopic fractionation at high temperatures is unlikely to have produced the differences in mineral δ^7Li observed in the Hannuoba peridotites.

6.2.2. Diffusion-induced isotopic fractionation during peridotite–melt interaction

Alkali elements have been reported to diffuse through silicate melts more than an order of magnitude faster than REE at magmatic temperatures (Nakamura and Kushiro, 1998; Mungall, 2002). The diffusivity of alkalis in silicate melts increases with decreasing ionic radii. Li is, therefore, one of the fastest diffusing elements in silicate melts. Because the diffusion rate of D_{6Li} is 1.034 times greater than that for D_{7Li} (Richter et al., 2003), large Li isotopic fractionations can be produced by diffusion during magmatic processes (Lundstrom et al., 2005; Teng et al., 2006a; Jeffcoate et al., 2007; Rudnick and Ionov, 2007). Therefore, it is possible that the large inter- and intra-mineral isotopic fractionation observed here were produced through Li diffusion.

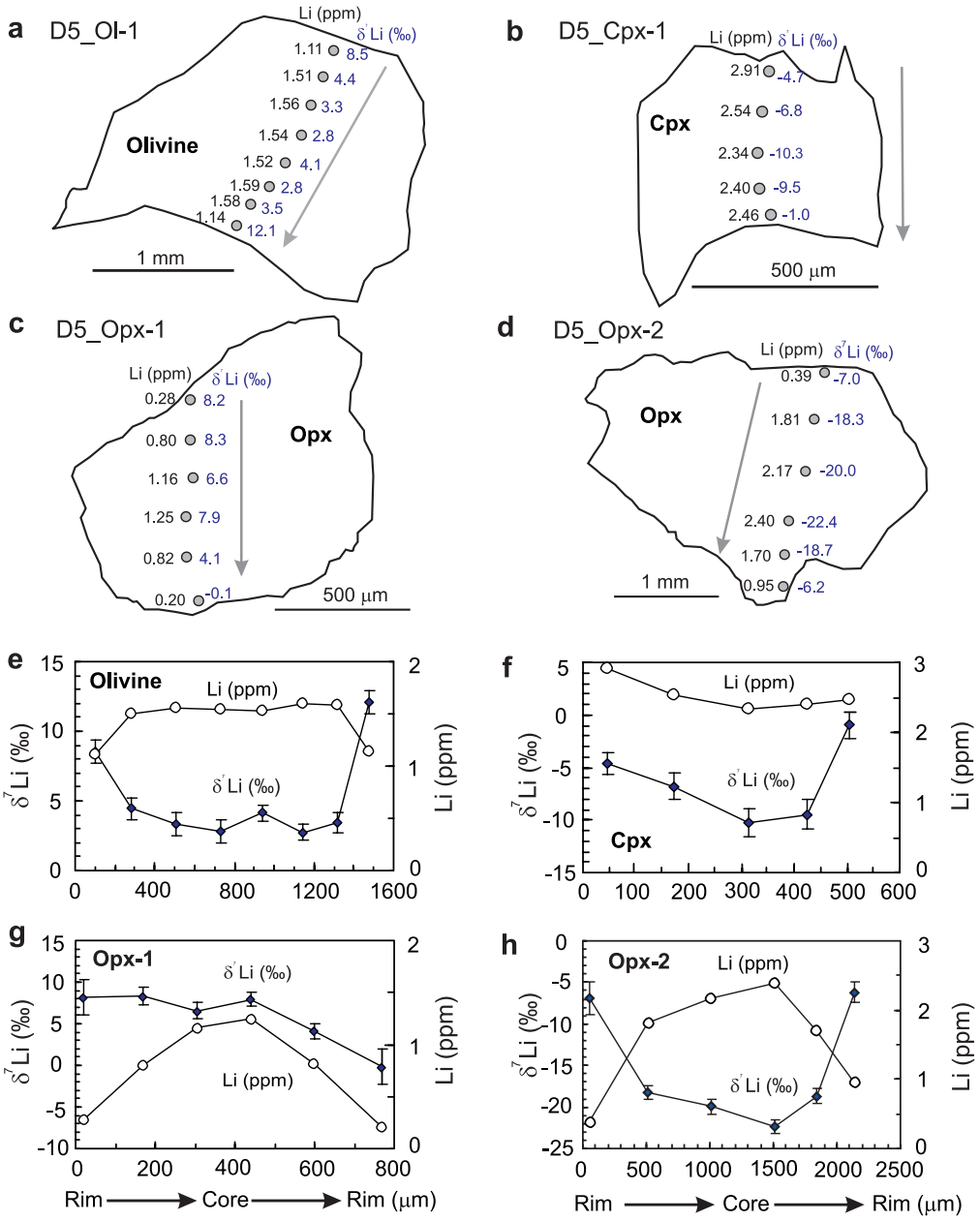

Fig. 7. Outlines of olivine (a), cpx (b), opx-1 (c), and opx-2 (d) crystals of the D5 showing the position of the Li isotopic and Li concentration measurements by SIMS. (e), (f), (g), and (h) are corresponding plots of Li isotope and concentration as profiles across these crystals.

Recent modeling of diffusion-induced isotopic fractionation generally assumes ingress of Li into rocks and minerals from a source of Li, such as Li diffusing into peridotite from Li-rich melt (basaltic magmas) (Lundstrom et al., 2005), or Li diffusing into amphibolite country rocks of Li-rich pegmatite (Teng et al., 2006a). In the case of Li addition to peridotites, the mantle minerals first become enriched in ^{6}Li because of its greater diffusion rate than ^{7}Li, leading to low δ^{7}Li relative to the source of Li. This mechanism has been used to explain the low δ^{7}Li in cpx from peridotite xenoliths from far-east Russia (Rudnick and Ionov, 2007) and Li isotope zonation in mineral phases of peridotites from southern Siberia and Mongolia (Jeffcoate et al., 2007). The above diffusive ingress of Li may also account for the observations of isotopically heavy cores with lower Li concentrations than the light rims of minerals.

In this study, we find a reverse sense of Li concentration and isotopic profiles in olivine and opx grains, i.e., isotopically heavy rims with lower Li concentrations than the light cores (Figs. 6 and 7). This may suggest diffusive flux of Li from the minerals into metasomatic melts. However, coexisting cpx grains from D4 (Fig. 6d) and D5 (Fig. 7f) show zonation of Li concentrations with edges higher than the cores. This observation indicates ingress of Li from melts. In theory, the diffusive ingress of Li into cpx would generate isotopic fractionation, resulting in isotopically light rims as observed by Jeffcoate et al. (2007). However, the cpx grains examined here have isotopically heavy rims and light cores

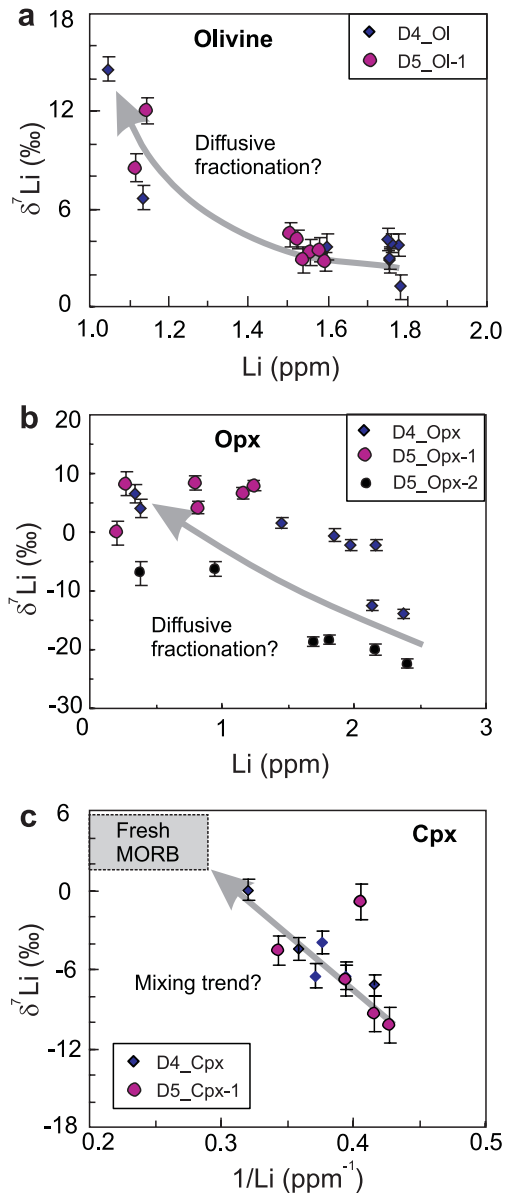

Fig. 8. Li isotopic composition versus Li concentration for (a) olivines, (b) opx, and (c) cpx based on SIMS data. See text for discussion.

(Figs. 6d and 7f), implying a complex flux of Li into cpx grains, rather than a simple diffusion process. There may be several ways to explain the observations:

(1) Simple diffusive process: Li diffusion from olivine and opx into melt, and meanwhile Li ingress into cpx from melt during peridotite–melt interaction.
(2) Differential diffusion of Li isotopes within the melt phase, a combined process of alkali diffusion and melt extraction, which allows larger Li concentration gradients to be developed and thus produces larger isotopic fractionations than simple diffusion models (Lundstrom et al., 2005). This model was used to explain the observations of very low δ^7Li in cpx in recent studies (Lundstrom et al., 2005; Jeffcoate et al., 2007; Rudnick and Ionov, 2007).
(3) Two-stage diffusive process of Li. At an earlier stage, the peridotites were modified by low δ^7Li fluid/melts related to oceanic crustal recycling. At a later stage, these rocks experienced modification via peridotite–asthenospheric melt interaction.

If the observations of Li elemental and isotopic zonation are produced via simple diffusion of Li between minerals and melt (#1, above), both olivine and opx should have higher δ^7Li values than the upper mantle value of ~3.5‰ (Jeffcoate et al., 2007) or ~4 ± 2‰ (Tomascak, 2004; Rudnick and Ionov, 2007), because their low Li concentrations at the rims indicate Li flux from crystals to melt, which would conceivably lead to an increase in δ^7Li in the mineral phases. However, the low δ^7Li values in olivine cores (some < 3‰) and opx cores (most < 0‰) preclude this possibility. Furthermore, diffusive ingress of Li into cpx, evidenced by the high Li concentrations at the rims, would lead to isotopically light rims, which is contrary to the observations (Figs. 6d and 7f).

It is also difficult to explain some of the observations using the second hypothesis (#2, above). According to the alkali diffusion and melt extraction model (Lundstrom et al., 2005), large changes in δ^7Li as a function of distance can be created. Such a model may account for the observations of Li isotopic variations in the Trinity ophiolite (northern California). However, the large Li isotopic variations observed in the Trinity ophiolite are across three transects ranging from 10s of centimeters to 1000s of centimeters, comprising several lithologic sequences from dunite to harzburgite to spinel lherzolite to plagioclase lherzolite (Lundstrom et al., 2005) rather than a mineral crystal of 1 or 2 mm. Using the Li diffusion data of cpx ($D = 3.9 \times 10^{-13}$ m^2 s^{-1} at 1000 °C; Coogan et al., 2005) and the β value (0.215) of Richter et al. (2003), the δ^7Li in a 2 mm cpx would decrease from +2.8‰ to −10‰, which is similar to the values observed in cpx in the Hannuoba xenoliths. However, the *in situ* data for pyroxenes in these xenoliths show some very low δ^7Li (~−22‰, Fig. 7h). On the other hand, the higher Li concentrations in opx and cpx cores (most > 2 ppm) than "normal" mantle peridotite (<2 ppm; Seitz and Woodland, 2000; Jeffcoate et al., 2007) cannot be well explained by the diffusion–extraction model. The very low δ^7Li melts produced in the model would have low Li concentrations due to melt extraction processes (see Fig. 9 in Lundstrom et al., 2005), and thus would drive Li concentrations in the peridotite minerals to lower values than the upper mantle. Consequently, the diffusion–extraction model may explain the observations of Li isotopic variations in the ophiolite of Lundstrom et al. (2005), but it may not be the best explanation of the observations in this study.

Fig. 9 is a schematic diagram showing the effects of the two-stage diffusive process (model #3 above). Before the diffusive ingress of Li into minerals from fluid/melts, the minerals in the mantle peridotites are in Li and Li isotopic composition equilibrium, similar to those of the normal upper mantle (Seitz and Woodland, 2000; Jeffcoate et al., 2007; Fig. 9a). Isotopically light peridotite minerals may be formed by the interaction between peridotite and low δ^7Li fluid/melts (e.g., δ^7Li = ~−9‰ to −11‰; Zack

et al., 2003). Both SIMS and ICP-MS data show that the minerals studied here have higher Li concentrations than the upper mantle, which requires that the low δ^7Li fluid/melts have higher Li concentrations than the upper mantle (Fig. 9b). The fluid/melts with the above characteristics could be derived from subducted oceanic crust. Meanwhile, low δ^7Li fluid/melt–peridotite interaction can also account for the bulk δ^7Li of the peridotites (<2.5‰, Table 3), which is lower than the upper mantle value of ~3.5‰ (Jeffcoate et al., 2007).

The elemental and isotopic profiles of Li in olivine and pyroxene grains indicate that the late-stage melts that infiltrated the peridotites might have originated from the asthenosphere (Fig. 9c). During asthenospheric melt–peridotite interaction, the isotopically light minerals with high Li concentrations might be the Li source. Since ^{6}Li will leave the mineral rims first (higher diffusivity), the olivine and opx crystals thus possess isotopically heavy rims with lower Li concentrations than their light cores (Figs. 6 and 7). This diffusive process is reinforced by the negative correlation of δ^7Li with Li concentrations in olivine and opx grains (Fig. 8a and b). The elemental and isotopic zonation of cpx (Figs. 6d and 7f) can also be explained by the asthenospheric melt–peridotite interaction. The high Li concentrations at the cpx rims may reflect the decrease of temperature during the crystallization of cpx, because elemental mineral–melt partition coefficients increase with decreasing temperature. As an alternative to the above explanation, the high Li concentrations at the cpx rims can also be related to the preferable enrichment of Li in cpx relative to olivine during the mafic silicate melt metasomatism (Seitz and Woodland, 2000; Woodland et al., 2004). The δ^7Li values of cpx may increase via mixing with asthenospheric melt, leading to isotopically heavier rims than the cores. The linear trend between δ^7Li and 1/Li (the inverse of Li concentrations) in cpx grains may indicate this mixing process (Fig. 8c).

7. CONCLUSION

Large Li elemental and isotopic disequilibria within and between mantle minerals from the Hannuoba spinel lherzolites have been observed in this study. These observations suggest

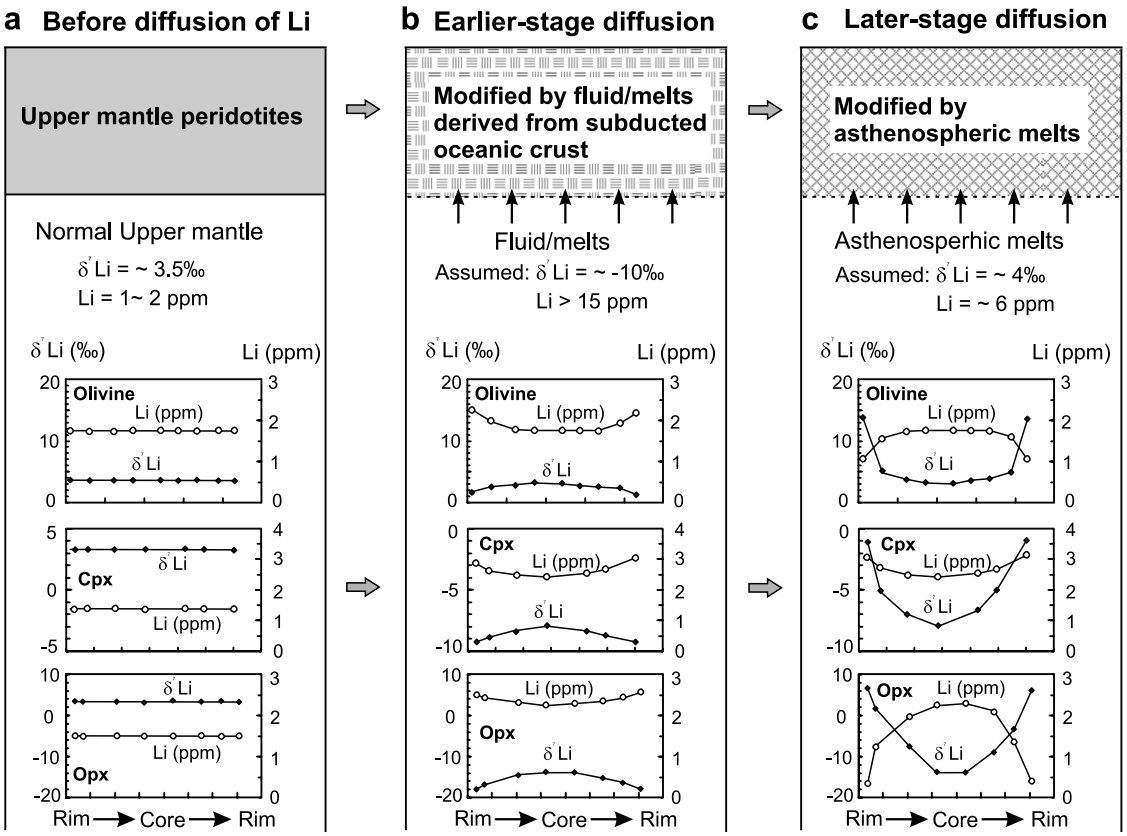

Fig. 9. Schematic diagram showing the effects of two-stage diffusive process of Li isotopes during the fluid/melt–rock interaction, after the schematic diagram of trace element diffusion of Nakamura and Kushiro (1998, Fig. 12). (a) Before the diffusive ingress of Li into minerals, the Li concentrations and isotopic compositions in the mantle peridotites are homogeneous, and similar to those of the normal upper mantle (Seitz and Woodland, 2000; Jeffcoate et al., 2007). (b) The early-stage diffusive ingress of Li into peridotite minerals from metasomatic fluid/melts, with higher Li concentrations and lower δ^7Li values (Zack et al., 2003) than those of the upper mantle, leads to an increase in Li concentration and decrease in δ^7Li in the minerals. Therefore, the peridotite minerals could develop zonation, with higher Li concentrations and lower δ^7Li values at the rim than those in the core, as observed in the cores of the minerals in this study. (c) The later-stage diffusive process of Li during the interaction between previously modified peridotites and asthenospheric melts. These melts have lower Li concentrations and higher δ^7Li values than those of the earlier-stage metasomatic agents, which results in the observations of lower Li concentrations and higher δ^7Li values at the rims of the minerals.

that the Hannuoba xenoliths have experienced two-stage metasomatism involving mafic silicate melts. The low δ^7Li values and high Li concentrations of bulk and individual minerals suggest that the early-stage metasomatic agents had low δ^7Li and high Li concentrations, due to the derivation from subducted, altered oceanic crust, which previously experienced devolatilization in the forearc, and that the later-stage metasomatic melts were derived from the asthenosphere.

Diffusive fractionation of Li isotopes during peridotite–melt interaction played an important role in producing inter- and intra-mineral differences in Li concentration and isotopic composition in the mantle peridotites. Thus, the Hannuoba peridotites have recorded multiple-stage melt–rock interactions in the considerably thinned lithospheric mantle and the Li data presented here provide clear evidence for the existence of such an effect beneath the North China Craton.

ACKNOWLEDGMENTS

We are very grateful to A. Makishima for his help at setting up Li isotope analysis by MC-ICP-MS, to T. Moriyama and C. Sakaguchi for their technical support in PML and to A. Ishikawa for his supply of SIMS standard materials from Solomon island. We thank Bjorn Mysen for the editorial encouragement and patience. The manuscript was considerably improved by the thoughtful comments and suggestions of Bjorn Mysen, James Brenan, Paul Tomascak and an anonymous reviewer. Gray Bebout and Bence Paul are thanked for their considerable efforts in improving the English expression. This research was financially supported by the Natural Science Foundation of China (40534022 and 40503004), the Knowledge Innovation Program of the Chinese Academy of Sciences (KZCX2-YW-103) and the program of COE-21 designated to the Institute for Study of the Earth's Interior, Okayama University, Japan.

APPENDIX A

Estimated mineral mode (%) and major elemental compositions in Hannuoba peridotites

	Sample				
	D1	D2	D3	D4	D5
Mode					
Olivine	66	65	60	55	63
Opx	24	23	30	30	20
Cpx	9	10	8	13	15
Spinel	1	2	2	2	2
SiO_2	44.52	44.62	45.35	45.93	45.05
TiO_2	0.15	0.10	0.10	0.10	0.12
Al_2O_3	2.42	2.90	3.05	3.30	2.67
Cr_2O_3	0.18	0.41	0.41	0.40	0.57
MgO	41.53	40.60	40.15	38.51	40.09
CaO	2.00	2.23	1.84	2.87	3.22
MnO	0.12	0.15	0.13	0.10	0.12
FeO	8.97	8.54	8.29	7.92	7.56
NiO	0.26	0.27	0.29	0.24	0.26
Na_2O	0.19	0.19	0.18	0.26	0.27
Total	100.3	100.0	99.8	99.6	99.9
Mg#	89.3	89.5	89.7	89.7	90.5

Abbreviations: opx, orthopyroxene; cpx, clinopyroxene. Mg# = 100 × molar Mg/(Mg + Fe).

APPENDIX B

Trace element analysis of JB3 standard

	Meas. (ppm)	1σ	n	RSD (%)	Ref. (ppm)	R.D. (%)
Li[a]	7.35	0.13	5	1.7	7.29	0.9
Li	7.31	0.27	5	3.7	7.28	0.4
Rb	14.2	0.3	5	2.4	14	1.7
Ba	243	3	5	1.3	239	1.8
Th	1.30	0.03	5	2.0	1.30	−0.4
U	0.480	0.007	5	1.5	0.480	0.1
La	8.19	0.06	5	0.8	8.12	0.8
Ce	21.5	0.1	5	0.7	20.9	0.7
Pb	4.87	0.06	5	1.2	4.85	0.3
Pr	3.16	0.05	5	1.7	3.14	0.6
Sr	419	4	5	0.9	414	1.3
Nd	16.0	0.1	5	0.6	15.9	0.8
Sm	4.35	0.06	5	1.4	4.17	4.4
Eu	1.34	0.00	5	0.1	1.31	2.2
Gd	4.76	0.04	5	0.8	4.77	−0.3
Tb	0.754	0.008	5	1.1	0.741	1.8
Dy	4.70	0.05	5	1.1	4.66	0.9
Y	23.7	0.3	5	1.3	23.1	2.8
Ho	0.954	0.005	5	0.5	0.949	0.6
Er	2.71	0.01	5	0.5	2.69	0.6
Tm	0.381	0.006	5	1.5	0.380	0.4
Yb	2.51	0.02	5	0.7	2.50	0.5
Lu	0.382	0.005	5	1.4	0.377	1.4

n, number of analyses; Meas., measured value; RSD, relative standard deviation; Ref., reference values; R.D., relative difference between measured and reference values.

[a] This value was determined by Li-ID method (Moriguti et al., 2004) and other values by Sm-ID method (Makishima and Nakamura, 2006).

APPENDIX C

Operating condition of MC-ICP-MS and desolvating nebulizer system

Plasma condition	
Plasma RF power/W	1200
Argon gas flow rate/l min^{-1}	
Cool gas	15
Auxiliary gas	0.8
Nebulizer gas	0.9
Desolvator condition	
Sweep gas (l min^{-1})	7.2
Nitrogen gas (ml min^{-1})	2
Sample uptake rate (μl min^{-1})	50

REFERENCES

Anders E. and Grevesse N. (1989) Abundances of the elements: meteoritic and solar. *Geochim. Cosmochim. Acta* **53**, 197–214.

Brenan J. M., Neroda E., Lundstrom C. C., Shaw H. F., Ryerson F. J. and Phinney D. L. (1998a) Behaviour of boron, beryllium and Lithium during melting and crystallization: constraints

from mineral–melt partitioning experiments. *Geochim. Cosmochim. Acta* **62**, 2129–2141.

Brenan J. M., Ryerson F. J. and Shaw H. F. (1998b) The role of aqueous fluids in the slab-to-mantle transfer of boron, beryllium, and lithium during subduction: experiments and models. *Geochim. Cosmochim. Acta* **62**, 3337–3347.

Brey G. P. and Köhler T. (1990) Geothermobarometry in four-phase lherzolites II. New thermobarometers, and practical assessment of existing thermobarometers. *J. Petrol.* **31**, 1353–1378.

Bryant C. J., Chappell B. W., Bennett V. C. and McCulloch M. T. (2004) Lithium isotopic composition of the New England Batholith: correlations with inferred source rock compositions. *Trans. R. Soc. Edinburgh Earth Sci.* **95**, 199–214.

Chan L. -H. and Frey F. A. (2003) Lithium isotope geochemistry of the Hawaiian plume: results from the Hawaii Scientific Drilling Project and Koolau volcano. *Geochem. Geophys. Geosyst.* **4**, doi:10.1029/2002GC000365.

Chan L.-H., Alt J. C. and Teagle D. A. H. (1996) Alteration of the upper 1.8 kilometers of oceanic crust: a lithium isotope record at ODP Site 504B. *Trans. Am. Geophys. Union* **77**, F805.

Chan L.-H., Alt J. C. and Teagle D. A. H. (2002a) Lithium and lithium isotope profiles through the upper oceanic crust: a study of seawater-basalt exchange at ODP Sites 504B and 896A. *Earth Planet. Sci. Lett.* **201**, 187–201.

Chan L.-H., Edmond J. M. and Thompson G. (1993) A lithium isotope study of hot-springs and metabasalts from midocean ridge hydrothermal systems. *J. Geophys. Res.* **98**, 9653–9659.

Chan L.-H., Edmond J. M., Thompson G. and Gillis K. (1992) Lithium isotopic composition of submarine basalts-implications for the lithium cycle in the oceans. *Earth Planet. Sci. Lett.* **108**, 151–160.

Chan L.-H., Leeman W. P. and You C.-F. (1999) Lithium isotopic composition of Central American Volcanic Arc lavas: implications for modification of subarc mantle by slab-derived fluids. *Chem. Geol.* **160**, 255–280.

Chan L.-H., Leeman W. P. and You C.-F. (2002b) Lithium isotopic composition of Central American volcanic arc lavas: implications for modification of subarc mantle by slab-derived fluids: correction. *Chem. Geol.* **182**, 293–300.

Chen S. H., O'Reilly S. Y., Zhou X. H., Griffin W. L., Zhang G. H., Sun M., Feng J. L. and Zhang M. (2001) Thermal and petrological structure of the lithosphere beneath Hannuoba, Sino-Korean Craton, China: evidence from xenoliths. *Lithos* **56**, 267–301.

Coogan L. A., Kasemann S. A. and Chakraborty S. (2005) Rates of hydrothermal cooling of new oceanic upper crust derived from lithium-geospeedometry. *Earth Planet. Sci. Lett.* **240**, 415–424.

Decitre S., Deloule E., Reisberg L., James R. E., Agrinier P. and Mevel C. (2002) Behaviour of Li and its isotope during serpentinization of oceanic peridotites. *Geochem. Geophys. Geosys.* **3**, 2001GC000187.

Elliott T., Jeffcoate A. and Bouman C. (2004) The terrestrial Li isotope cycle: light-weight constrains on mantle convection. *Earth Planet. Sci. Lett.* **220**, 231–245.

Fan W. M., Zhang H. F., Baker J., Jarvis K. E., Mason P. R. D. and Menzies M. A. (2000) On and off the north China craton: where is the Archaean keel? *J. Petrol.* **41**, 933–950.

Gao S., Rudnick R. L., Carlson R. W., McDonough W. F. and Liu Y. S. (2002) Re-Os evidence for replacement of ancient mantle lithosphere beneath the North China Craton. *Earth Planet. Sci. Lett.* **198**, 307–322.

Griffin W. L., Zhang A. D., O'Reilly S. Y. and Ryan C. G. (1998) Phanerozoic evolution of the lithosphere beneath the Sino-Korean Craton. In *Mantle Dynamics and Plate Interactions in East Asia* (eds. M. F. J. Flower, S. L. Chung, C. H. Lo and T. Y. Lee). American Geophysical Union, Washington, DC, Geodynamics Series 27, pp. 107–126.

James R. H. and Palmer M. R. (2000) The lithium isotope composition of international rock standards. *Chem. Geol.* **166**, 319–326.

Jeffcoate A. B., Elliott T., Kasemann S. A., Ionov D., Cooper K. and Brooker R. (2007) Li isotope fractionation in peridotites and mafic melts. *Geochim. Cosmochim. Acta* **71**, 202–218.

Kobayashi K., Tanaka R., Moriguti T., Shimizu K. and Nakamura E. (2004) Lithium, boron, and lead isotope systematics of glass inclusions in olivines from Hawaiian lavas: evidence for recycled components in the Hawaiian plume. *Chem. Geol.* **212**, 143–161.

Liu D. Y., Nutman A. P., Compston W., Wu J. S. and Shen Q. H. (1992) Remnants of 3800 Ma crust in the Chinese part of the Sino-Korean craton. *Geology* **20**, 339–342.

Liu Y. S., Gao S., Lee C.-T. A., Hu S. H., Liu X. M. and Yuan H. L. (2005) Melt–peridotite interactions: links between garnet pyroxenite and high-Mg# signature of continental crust. *Earth Planet. Sci. Lett.* **234**, 39–57.

Lundstrom C. C., Chaussidon M., Hsui A. T., Kelemen P. and Zimmerman M. (2005) Observations of Li isotopic variations in the Trinity Ophiolite: evidence for isotopic fractionation by diffusion during mantle melting. *Geochim. Cosmochim. Acta* **69**, 735–751.

Makishima A. and Nakamura E. (2006) Determination of major, minor and trace elements in silicate samples by ICP-QMS and ICP-SFMS applying isotope dilution-internal standardisation (ID-IS) and multi-stage internal standardisation. *Geostand. Geoanal. Res.* **30**, 245–271.

McDonough W. F. and Sun S. S. (1995) The composition of the Earth. *Chem. Geol.* **120**, 223–253.

Menzies M. A., Fan W. M. and Zhang M. (1993) Palaeozoic and Cenozoic lithoprobes and the loss of >120 km of Archaean lithosphere, Sino-Korean craton, China. In *Magmatic Processes and Plate Tectonics*, vol. 76 (eds. H. M. Prichard, T. Alabaster, N. B. W. Harris and C. R. Neary). Spec. Pub., Geol. Soc. London, pp. 71–81.

Moriguti T. and Nakamura E. (1998a) Across-arc variation of Li isotopes in lavas and implications for crust/mantle recycling at subduction zones. *Earth Planet. Sci. Lett.* **163**, 167–174.

Moriguti T. and Nakamura E. (1998b) High-yield lithium separation and the precise isotopic analysis for natural rock and aqueous samples. *Chem. Geol.* **145**, 91–104.

Moriguti T., Makishima A. and Nakamura E. (2004) Determination of Lithium contents in silicates by isotope dilution ICP-MS and its evaluation by isotope dilution thermal ionisation mass spectrometry. *Geostand. Geoanal. Res.* **28**, 371–382.

Mungall J. E. (2002) Empirical models relating viscosity and tracer diffusion in magmatic silicate melts. *Geochim. Cosmochim. Acta* **66**, 125–143.

Nakamura E. and Kushiro I. (1998) Trace element diffusion in jadeite and diopside melts at high pressures and its geochemical implication. *Geochim. Cosmochim. Acta* **62**, 3151–3160.

Nakamura E., Makishima A., Moriguti T., Kobayashi K., Sakaguchi C., Yokoyma T., Tanaka R., Kuritani T. and Takei H. (2003) Comprehensive geochemical analyses of small amounts (<100 mg) of extraterrestrial samples for the analytical competition related to the sample return mission MUSES-C. In *Asteroidal Sample Preliminary Examination Team, Inst. Space and Astron. Sci. Report. SP No. 16* (eds. I. Kushiro, A. Fujiwara and H. Yano), Sagamihara, Japan, pp. 49–101.

Nishio Y., Nakai S. i., Yamamoto J., Sumino H., Matsumoto T., Prikhod'Ko V. S. and Arai S. (2004) Lithium isotopic systematics of the mantle-derived ultramafic xenoliths: implications for EM1 origin. *Earth Planet. Sci. Lett.* **217**, 245–261.

Ottolini L., Fèvre B. L. and Vannucci R. (2004) Direct assessment of mantle boron and lithium contents and distribution by SIMS analyses of peridotite minerals. *Earth Planet. Sci. Lett.* **228**, 19–36.

Richter F. M., Davis A. M., Depaolo D. J. and Watson E. B. (2003) Isotope fractionation by chemical diffusion between molten basalts and rhyolite. *Geochim. Cosmochim. Acta* **67**, 3905–3923.

Rudnick R. L. and Ionov D. A. (2007) Lithium elemental and isotopic disequilibrium in minerals from peridotite xenoliths from far-east Russia: product of recent melt/fluid–rock reaction. *Earth Planet. Sci. Lett.* **256**, 278–293.

Rudnick R. L., Gao S., Ling W. L., Liu Y. S. and McDonough W. F. (2004) Petrology and geochemistry of spinel peridotite xenoliths from Hannuoba and Qixia, North China Craton. *Lithos* **77**, 609–637.

Seitz H.-M. and Woodland A. B. (2000) The distribution of lithium in peridotitic and pyroxenitic mantle lithologies-an indicator of magmatic and metasomatic processes. *Chem. Geol.* **166**, 47–64.

Seitz H.-M., Brey G. P., Lahaye Y., Durali S. and Weyer S. (2004) Lithium isotopic signatures of peridotite xenoliths and isotopic fractionation at high temperature between olivine and pyroxenes. *Chem. Geol.* **212**, 163–177.

Song Y. and Frey F. A. (1989) Geochemistry of peridotite xenoliths in basalt from Hannuoba, eastern China: implications for subcontinental mantle heterogeneity. *Geochim. Cosmochim. Acta* **53**, 97–113.

Tanaka R. and Nakamura E. (2005) Boron isotopic constraints on the source of Hawaiian shield lavas. *Geochim. Cosmochim. Acta* **69**, 3385–3399.

Tang Y. J., Zhang H. F. and Ying J. F. (2007) Review of the lithium isotope system as a geochemical tracer. *Int. Geol. Rev.* **49**, 274–388.

Teng F.-Z., McDonough W. F., Rudnick R. L. and Walker R. J. (2006a) Diffusion-driven extreme lithium isotopic fractionation in country rocks of the Tin Mountain pegmatite. *Earth Planet. Sci. Lett.* **243**, 701–710.

Teng F.-Z., McDonough W. F., Rudnick R. L., Dalpé C., Tomascak P. B., Chappell B. W. and Gao S. (2004) Lithium isotopic composition and concentration of the upper continental crust. *Geochim. Cosmochim. Acta* **68**, 4167–4178.

Teng F.-Z., McDonough W. F., Rudnick R. L., Walker R. J. and Sirbescu M.-L. C. (2006b) Lithium isotopic systematics of granites and pegmatites from the Black Hill, South Dakota. *Am. Mineral.* **91**, 1488–1498.

Tomascak P. B. (2004) Developments in the understanding and application of lithium isotopes in the Earth and planetary sciences. In *Geochemistry of Non-traditional Stable Isotope: Reviews in Mineralogy and Geochemistry*, vol. 55 (eds. C. M. Johnson, B. I. Beard and F. Albarede). Mineral Soc. Am., Washington, DC, pp. 153–195.

Tomascak P. B., Ryan C. G. and Defant M. J. (2000) Lithium isotope evidence for light element decoupling in the Panama subarc mantle. *Geology* **28**, 507–510.

Tomascak P. B., Tera F., Helz R. and Walker R. J. (1999) The absence of lithium isotope fractionation during basalt differentiation: new measurements by multicollector sector ICP-MS. *Geochim. Cosmochim. Acta* **63**, 907–910.

Tomascak P. B., Widom E., Benton L. D., Goldstein S. L. and Ryan J. G. (2002) The control of lithium budgets in island arcs. *Earth Planet. Sci. Lett.* **196**, 227–238.

Woodland A. B., Seitz H.-M. and Yaxley G. M. (2004) Varying behaviour of Li in metasomatised spinel peridotite xenoliths from western Victoria, Australia. *Lithos* **75**, 55–66.

Wunder B., Meixner A., Romer R. L. and Heinrich W. (2006) Temperature-dependent isotopic fractionation of lithium between clinopyroxene and high-pressure hydrous fluids. *Contrib. Mineral. Petrol.* **151**, 112–120.

Xu Y. G. (2002) Evidence for crustal components in the mantle and constrains on crustal recycling mechanisms: pyroxenite xenoliths from Hannuoba, North China. *Chem. Geol.* **182**, 301–322.

Yang J. H., Wu F. Y. and Wilde S. A. (2003) A review of the geodynamic setting of large-scale Late Mesozoic gold mineralization in the North China craton: an association with lithospheric thinning. *Ore Geol. Rev.* **23**, 125–152.

Zack T., Tomascak P. B., Rudnick R. L., Dalpé C. and McDonough W. F. (2003) Extremely light Li in orogenic eclogites: the role of isotope fractionation during dehydration in subducted oceanic crust. *Earth Planet. Sci. Lett.* **208**, 279–290.

Zhang H. F. (2005) Transformation of lithospheric mantle through peridotite–melt reaction: a case of Sino-Korean craton. *Earth Planet. Sci. Lett.* **237**, 768–780.

Zhang H. F. and Sun M. (2002) Geochemistry of Mesozoic basalts and mafic dikes, southeastern north China craton, and tectonic implications. *Int. Geol. Rev.* **44**, 370–382.

Zhang H. F., Sun M., Zhou X. H., Zhou M. F., Fan W. M. and Zheng J. P. (2003) Secular evolution of the lithosphere beneath the eastern North China Craton: evidence from Mesozoic basalts and high-Mg andesites. *Geochim. Cosmochim. Acta* **67**, 4373–4387.

Zhao G. C., Wilde S. A., Cawood P. A. and Sun M. (2001) Archean blocks and their boundaries in the North China Craton: lithological, geochemical, structural and P–T path constraints and tectonic evolution. *Precambrian Res.* **107**, 45–73.

Zhou X. H. and Armstrong R. L. (1982) Cenozoic volcanic rocks of eastern China-secular and geographic trends in chemistry and strontium isotopic composition. *Earth Planet. Sci. Lett.* **58**, 301–329.

Associate editor: Bjorn Mysen